High Energy Physics and Nuclear Physics

Volume 19, Number 2

# Geometric and Fragmentation Effects in Leading Particle Rapidity Distributions for High-energy p-A Collisions

Liu Qingjun and Zhao Weiqin

(Institute of High Energy Physics, The Chinese Academy of Sciences, Beijing, China)

**Based on the interacting gluon model (IGM), leading particle rapidity distributions for 100 GeV p+Ag collisions are calculated and compared with experimental data. The results are in agreement with data obtained from using a more sophisticated collision geometry and including final-state fragmentation process.**

**Key words: stopping power, fragmentation effect, geometric effect.**

## 1. INTRODUCTION

Energy density of nuclear matter formed in the early stage of a nucleus-nucleus collision is needed to determine if quark-gluon-plasma is produced in the collision. The energy density is closely related to the nuclear stopping power. As a reliable guide to the study of nuclear stopping power in nucleus-nucleus us (A-A) collisions, the study of nuclear stopping power in high-energy proton-nucleus (p-A) processes has been an energetically discussed topic. Recently, G.N. Fowler *et al.* [1] extended the interacting gluon model for high-energy N-N process to study nuclear stopping power in 100 GeV p+Ag and Au+Au collisions. In [1–3], the energy loss in soft N-N interactions is assumed to be caused by gluon-gluon interactions, and the high-energy p-A and A-A processes are considered a superposition of multiple scatterings of gluons. Based on these assumptions, the authors investigated the energy deposition in the central rapidity region and calculated the leading particle rapidity

Received on April 13, 1994. Partly Supported by the National Natural Science Foundation of China.

distributions for high-energy p-A and A-A collisions. However, because this model does not take into account the final-state fragmentation effect, and the relation of collision geometry with the number of final-state gray particles is not well defined in high-energy p-A process, the calculated leading particle rapidity distributions deviate from the experimental data. Larger deviations appeared in peripheral collisions especially, showing that the IGM needs to be improved.

In this paper, after an introduction to the IGM, the final-state fragmentation effect is included in the model. Furthermore, the energy deposition process in high-energy p-A collisions is assumed to proceed via consecutive collisions of incident protons with nucleons in the target nucleus, and the improved IGM is applied to high-energy p-A collisions with two kinds of collision geometries. Then leading particle rapidity distributions for 100 GeV p+Ag collisions are calculated and compared with experimental data, from which the geometric and fragmentation effects in the distributions are studied.

## 2. LEADING PARTICLE RAPIDITY DISTRIBUTION AND THE IGM FOR THE HIGH-ENERGY N-N PROCESS

The IGM can be summarized as follows: assume that the PQCD predicted inequality $\sigma_{gg} \gg \sigma_{gq} \gg \sigma_{qq}$ with $\sigma_{gg}$, $\sigma_{gq}$, and $\sigma_{qq}$ being the interaction cross sections of gluon-gluon, gluon-quark, and quark-quark pairs, respectively, holds also in soft hadronic interactions. In the course of a high-energy N-N collision gluconic clouds interact strongly and produce minifireballs (MFs), which will form a central fireball (CF) in the central rapidity region and decay into final-state hadrons; the valence quarks (together with the gluons that did not interact) interact weakly, going through the central region and fragmenting into final-state hadrons in the fragmentation regions. Omitting this fragmentation effect, leading particle rapidity distribution in high-energy N-N collisions can be expressed as

$$\frac{dN}{Ndy} = x_L f_{\nu=1}(x_L). \tag{2.1}$$

where $x_L$ stands for the fraction of energy of the incident proton, which is carried by the leading particle. This fraction $x_L$, the leading particle rapidity $y$, and the rapidity $y_{Proj.}$ of the incident proton are related via the following expressions:

$$\begin{cases} x_L \equiv e^{-(\delta y)} \\ \delta y \equiv y_{Proj.} - y. \end{cases} \tag{2.2}$$

and $f_{\nu=1}(x_L)$ is formulated as

$$f_{\nu=1}(x_L) = \int_0^1 \int_0^1 dx dy \chi(x,y) \delta(1 - x_L - x). \tag{2.3}$$

here $x$ and $y$ are fractions of energy of the incident and target nucleons, which are carried by the interacting gluons. $\chi(x,y)$, being an energy distribution function for the $x$ and $y$ just mentioned, is deduced as

$$\begin{aligned} \chi(x,y) = \chi^0 & e^{-((x-\langle x\rangle)^2/2\langle x^2\rangle)} \\ & e^{-((y-\langle y\rangle)^2/2\langle y^2\rangle)} \\ & \theta(xy - K_{min}^2). \end{aligned} \tag{2.4}$$

Here $\chi^0$ is a normalization factor. There is a simple relation among moments $\langle x\rangle$, $\langle x^2\rangle$, and $\langle y\rangle$, $\langle y^2\rangle$ that is valid at high energy, namely

$$\langle x\rangle \approx \langle y\rangle \approx 2\langle x^2\rangle \approx 2\langle y^2\rangle \approx \alpha_0/\sigma_{NN}^{in}(s). \tag{2.5}$$

$K_{min}$ stands for the minimal inelasticity for high-energy N-N collisions, which is related to the lightest invariant mass of the possible central fireball and is defined as

$$K^2_{min} = M^2_0/s. \tag{2.6}$$

The $s$ in Eqs. (2.5) and (2.6) stands for the squared c.m. energy of the N-N system, whereas in Eq. (2.5) $\sigma^{in}_{NN}(s)$ is the inelastic cross section for the high-energy N-N process, and $\alpha_0$ is defined as

$$\alpha_0 = \alpha p^2_h / M^2_0. \tag{2.7}$$

where $\alpha$ is a phenomenological parameter related to the strong coupling constant, $p_h$ represents the fraction of the hadron energy attributed to gluons in hadron structure function [4], and $\alpha$ and $p^2_h$ appear in the form of product $\alpha p^2_h$ [1]. The definition of the invariant mass for the central fireball is

$$M = \sqrt{xys}. \tag{2.8}$$

From the preceding brief introduction, one can see that there are two basic input parameters in the IGM: $\alpha p^2_h$ and $M_0$.

## 3. COLLISION GEOMETRY FOR 100 GeV p+Ag COLLISIONS

Assuming that the impact parameter for p-A process is $b$ and there are an average of $n$ nucleons in A, which scatter inelastically with p, then as a function of $b$, $n$ is expressed as

$$n(b) = \sigma^{in}_{NN}(s) \int_{-\infty}^{+\infty} \rho(b,z)dz. \tag{3.1}$$

Averaged over the impact parameter, the probability for p to scatter inelastically with $\nu$ nucleons in nucleus A in the p-A process is

$$T(\nu) = \frac{\int n^\nu(b)e^{-n(b)}d^2b}{\nu!\sigma^{in}_{pA}(s)}. \tag{3.2}$$

$\rho(b,z)$ in Eq. (3.1) and $\sigma^{in}_{pA}(s)$ in Eq. (3.2) are the nucleon density and inelastic cross section, respectively, for p-A processes. One can have the following expressions:

$$\iint \rho(b,z)dzd^2b = A, \tag{3.3}$$

$$\sigma^{in}_{pA}(s) = \int (1 - e^{-n(b)})d^2b. \tag{3.4}$$

In this paper, $\rho(b,z)$ is taken from [5].

Experimentally, collision events are grouped into central and peripheral events, and their leading particle rapidity distributions are measured. In [1], referring to experimental data, the central collision event is simply defined as the event with $\nu \geq 6$ and the peripheral event with $\nu \leq 5$; therefore in 100 GeV p+Ag collisions the probability for the incident proton to scatter inelastically with $\nu$ nucleons in the target nucleus is

$$\begin{cases} T_{\text{central}}(\nu) = T(\nu)\theta(\nu - 5) \\ T_{\text{periph.}}(\nu) = T(\nu)\theta(6 - \nu). \end{cases} \tag{3.5}$$

On the other hand, there is a correlation distribution [6,7] between the number $\nu$ of the participant nucleons in the target nucleus and the number $N_g$ of the final-state gray particles, $P_\nu(N_g)$. To follow strictly the experimental conditions [8] for 100 GeV p+Ag collisions, the probability for the incident proton to scatter inelastically with $\nu$ nucleons in the target nucleus is obtained via

$$\begin{cases} T_{\text{central}}(\nu) = T(\nu) \sum\limits_{N_g>3} P_\nu(N_g) \\ T_{\text{periph.}}(\nu) = T(\nu) \sum\limits_{N_g<3} P_\nu(N_g), \end{cases} \tag{3.6}$$

Here the correlation distribution between $\nu$ and $N_g$ is from [6,7]:

$$P_\nu(N_g) = \binom{N_g + \nu - 1}{N_g} (1 - X)^\nu X^{N_g}, \tag{3.7}$$

and according to [8], for 100 GeV p+Ag collisions $X = 0.52$.

Judging from the preceding two collision geometries defined by Eqs. (3.5) and (3.6), there are noticeable differences in their classifications of central and peripheral collisions. In section five we will compare the results from the two considerations of the collision geometry and show that the latter is more reasonable than the former.

## 4. IMPROVEMENT ON THE IGM FOR THE HIGH-ENERGY p-A PROCESS

Using IGM, G. N. Fowler *et al.* calculated leading particle rapidity distributions in 100 GeV p+Ag collisions, and the results are in agreement with the data from global events. However, theoretical results deviate from experimental data both for the central collisions and for the peripheral collision events. For the peripheral collisions events and beam rapidity regions, especially, the deviation is larger. To explain the data, our improvement on the IGM is given in the following.

Generally speaking, not only do the gluon interactions influence the leading particle rapidity distributions, so does the fragmentation of valence quarks into final-state hadrons. When there is no way to differentiate the two kinds of contributions, we assume the data of leading particle rapidity distributions to be a summation of the two. Then, according to the data, the distribution of the lost fractions of energy of either the incident or the target nucleon is assumed to be uniform:

$$\chi_f(x) = 1, x \in (0,1], \tag{4.1}$$

Thus, in the improved IGM, the distribution of lost fractions of energy in N-N collisions is

$$\chi(x,y) = \chi_f^0 \chi_f(x) \chi_f(y) \theta(xy - K_{\min}^2), \tag{4.2}$$

where $x$ and $y$ are the lost fractions of energy of incident and target nucleons, after both of them have experienced the gluon interaction and final-state fragmentation. $\chi_f^0$ is a normalization factor.

For high-energy p-A collisions, Eq. (4.1) is also the distribution for the incident proton in its last collisions. For the collision in which only gluon interaction occurs and no final-state fragmentation is involved, the distribution is of the form given in Eq. (2.4).

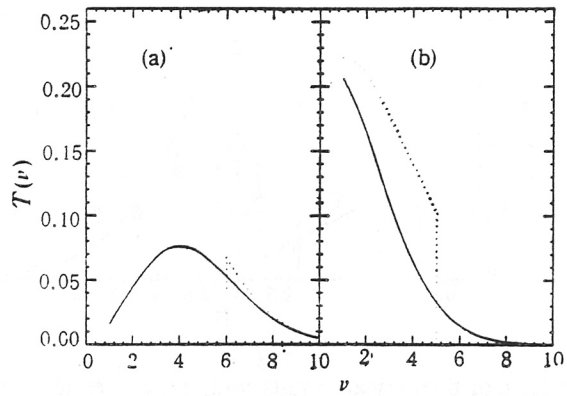


**Fig. 1**

Probability distribution $T(\nu)$ for p to collide with $\nu$ nucleons of Ag in high-energy p-Ag process ((a) central collisions; (b) peripheral collisions). Dotted lines and solid lines represent results corresponding to the first and second kinds of collision geometry, respectively.

Assuming that the high-energy p-A process is a number of consecutive p-N collisions, then, averaged over impact parameter $b$, the leading particle rapidity distribution can be expressed as

$$\frac{dN}{N\,dy} = x_L \frac{dN}{N dx_L} = x_L \sum_{\nu=1}^{A} T(\nu) f_\nu(x_L), \tag{4.3}$$

where $f_\nu(x_L)$ is a superposition of the distribution functions of the lost fractions of energy in $\nu$ p-N collisions:

$$f_\nu(x_L) = \chi_\nu^0 \int_0^1 dx_1 dy_1 \cdots \int_0^1 dx_\nu dy_\nu \prod_{i=1}^{\nu} \chi_i(x_i, y_i)^{p-N} \delta\left(x_L - \prod_{j=1}^{\nu} (1 - x_j)\right). \tag{4.4}$$

Here $\chi_i(x_i, y_i)^{p\text{-}N}$ is the distribution when the lost fractions of energy of the incident proton and the target nucleon are $x_i$ and $y_i$ in the $i$-th p-N collision:

$$\chi_i(x_i, y_i)^{p-N} = \chi_i^p(x_i)\chi_i^T(y_i)\theta(x_i y_i - K_{min}^2), \tag{4.5}$$

Here $\chi_i^p(x_i)$ and $\chi_i^T(y_i)$ are the distributions of the lost fractions of energy of the incident proton and the target nucleon in the $i$-th p-N collision. $\chi_\nu^0$ is a normalization factor. Because the incident proton will fragment only after the last (i.e., the $\nu$-th) collisions, the distribution of its lost fraction of energy should be different for the $\nu$-th collision and the collisions before, that is,

$$\chi_i^p(x_i) = \begin{cases} e^{-(x_i - \langle x_i \rangle)^2 / 2\langle x_i^2 \rangle}, i \in [1, \nu - 1] \\ \chi_f(x_i), \quad i = \nu. \end{cases} \tag{4.6}$$

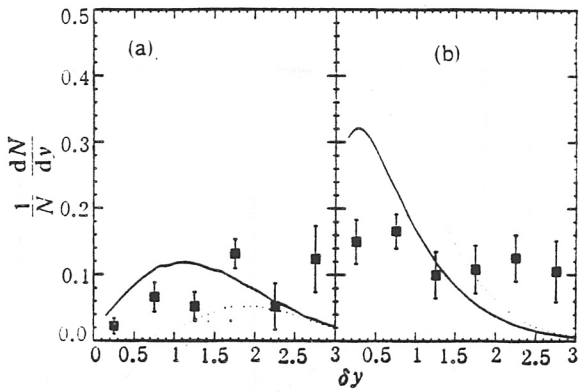


**Fig. 2**

A comparison of theoretical results with experimental data for leading particle rapidity distributions in 100-GeV p+Ag central (a) and peripheral (b) collisions with the final-state fragmentation effect not included in calculations. Dotted lines and solid lines represent results corresponding to the first and second kinds of collision geometry, respectively. Input parameters are: $\alpha p_h^2 = 0.06$ $(GeV)^2(fm)^2$, $M_0 = 0.35$ GeV.

Because the target nucleon experiences only one collision before its fragmentation, one obtains

$$\chi_i^T(y_i) = \chi_t(y_i). \tag{4.7}$$

Based on Eqs. (4.3)–(4.7) and using Eqs. (3.5) or (3.6), leading particle rapidity distributions in central or peripheral collisions can be calculated.

## 5. LEADING PARTICLE RAPIDITY DISTRIBUTIONS IN 100 GeV p+Ag COLLISIONS

Analyses of the two collision geometries are given in the following. Figure 1 shows the probability distributions $T(\nu)$ for p to collide with $\nu$ nucleons of Ag in high-energy p-Ag process. Dotted lines and solid lines represent results corresponding to the first and the second kinds of collision geometry, respectively. It is shown in Fig. 1 that either in peripheral collisions 1(a) or in central collisions 1(b) the results for $T(\nu)$ are very different for the two geometrical considerations. This difference originating in different collision geometries manifests itself in the leading particle rapidity distributions. In the following, it is demonstrated how the leading particle rapidity distributions are different in the two different collisions geometries.

Figures 2(a) and (b) display leading particle rapidity distributions using different collision geometries in central and peripheral collisions where the final-state fragmentation effect is omitted. Dotted lines and solid lines represent results corresponding to the first and second kinds of collision geometry, respectively. Compared to the results from the first collision geometry, the results from the second collision geometry are more compatible with the experimental data. However, in the preceding theoretical calculations the final-state fragmentation effect is not taken into account; thus further improvement is necessary to fit the data. Using the improved IGM that takes into account the final-state fragmentation effect, we calculated results for the leading particle rapidity distributions corresponding to the two collision geometries and compared with the data, and came to the same conclusion as mention previously. In the second kind of collision geometry, events are classified according to the number of final-state gray particles with the introduced distribution of $\nu$ for fixed $N_g$,

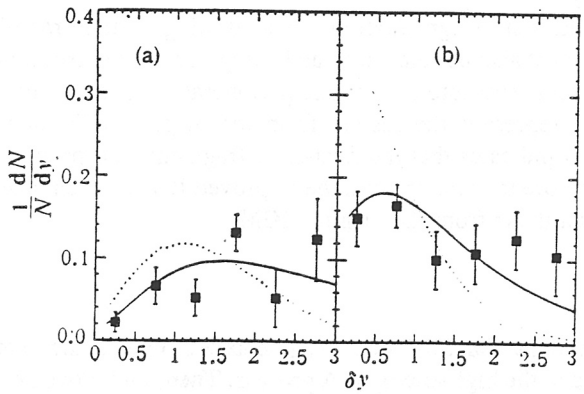


**Fig. 3**

A comparison of theoretical results with experimental data for leading particle rapidity distributions in 100-GeV p+Ag central (a) and peripheral (b) collisions with the use of the second kind of collision geometry in theoretical calculations. Dotted lines and solid lines represent results corresponding to the original IGM (not including the fragmentation effect) and the improved IGM (with the fragmentation effect included), respectively. Input parameters are the same as those in Fig. 2.

which is consistent with the method used in data analysis.

The leading particle rapidity distributions in central and peripheral collisions using the second collision geometry are shown in Figs. 3(a) and (b). Dotted lines and solid lines represent the results from the IGM (not including final-state fragmentation effect) and the improved IGM (including the effect). It can be seen that the final-state fragmentation effect is nontrivial; compared to the results not including the final-state fragmentation effect, the results from the improved IGM including the effect fit the data better. The explanation is that the effect makes the incident proton more stopped; therefore the corresponding leading particle rapidity distributions better approximate the data. Using the first

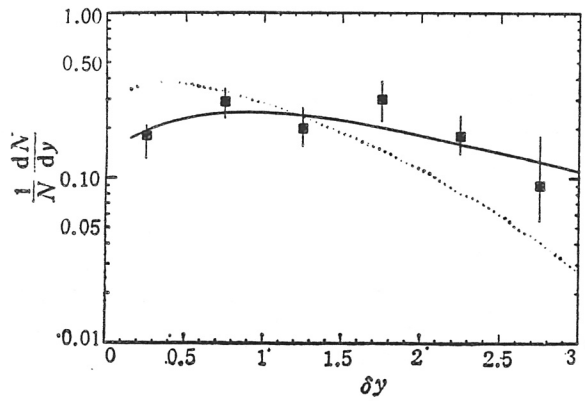


**Fig. 4**

A comparison of theoretical results with experimental data for leading particle rapidity distributions in 100-GeV p+Ag collisions. Dotted lines and solid lines represent results from the original IGM (not including the fragmentation effect) and the improved IGM (with the fragmentation effect included), respectively. Input parameters are the same as those in Fig. 2.

kind of collision geometry, our analysis leads to the same conclusion as when using the second kind of collision geometry.

To study the final-state fragmentation effect, leading particle rapidity distribution in 100 GeV p+Ag global events must also be calculated and compared with corresponding the experimental data, not classifying the total events into central and peripheral collision events, as shown in Fig. 4. Dotted lines and solid lines represent the results from the original IGM and from the improved IGM, respectively. Figure 4 indicates that the final-state fragmentation process leads to a stronger nuclear stopping power; therefore the results from the improved IGM, which takes into account this process, fit the data better than those from the original IGM.

## 6. CONCLUSION

Taking into account the final-state fragmentation effect, the interacting gluon model was improved and applied to the high-energy p-A process. Then, under two geometrical considerations for the high-energy p-A process and by using both the original and the improved IGM, leading particle rapidity distributions in 100 GeV p+Ag collisions were calculated and compared with the experimental data. In conclusion, geometric and fragmentation effects on leading particle rapidity distributions in the high-energy p-A process are nontrivial; when using a stricter collision geometry and taking into account the fragmentation effect, the experimental data are reproduced well.

## REFERENCES

[1] G. N. Fowler *et al.*, *Phys. Rev.*, **C40**(1989): p. 1219.
[2] G. N. Fowler *et al.*, *Phys. Rev. Lett.*, **55**(1985): p. 173.
[3] G. N. Fowler *et al.*, *Phys. Rev.*, **D35**(1987): p. 870.
[4] P. L'Heureux, B. Margolis, and P. Valin, *Phys. Rev.*, **D32**(1985): p. 1681.
[5] S. Date, M. Gyulassy, and H. Sumiyoshi, *Phys. Rev.* **D32**(1985): p. 619.
[6] B. Andersson, I. Otterlund, and E. Stenlund, *Phys. Lett.*, **B73**(1978): p. 343.
[7] M. K. Hegab and J. Hufner, *Phys. Lett.*, **B105**(1981): p. 103; *Nucl. Phys.*, **A384**(1982): p. 353.
[8] W. S. Toothacker *et al.*, *Phys. Lett.*, **B197**(1987): p. 295.